



ORIGINAL ARTICLE

# Numerical simulation of punching shear failure in recycled aggregate concrete slabs with steel fiber reinforcement

*Simulação numérica de ruptura por punção em lajes de concreto com agregado reciclado com reforço de fibra de aço*

Alana Helena Cara Siqueira<sup>a</sup> Marcela Gimenes<sup>a</sup> Osvaldo Luís Manzoli<sup>a</sup> Eduardo Alexandre Rodrigues<sup>a</sup> <sup>a</sup>Universidade Estadual Paulista, Departamento de Engenharia Civil e Ambiental, Bauru, SP, Brasil

Received 02 December 2022

Accepted 04 April 2023

**Abstract:** The use of construction waste as aggregate in the production of concrete is becoming a more frequent alternative due to the advantages associated with the sustainability aspect. Results obtained in experimental tests with recycled aggregate concrete suggest that mechanical properties such as elastic modulus, compressive, tensile and flexural strength tend to reduce with partial or total replacement of natural aggregate by recycled one. On the other hand, the use of steel fiber reinforcement can minimize the reduction of these properties, since the fibers tend to improve the material strength and ductility. This work proposes a numerical approach, seeking to better predict and understand the structural mechanical behaviors and failure patterns of reinforced recycled aggregate concrete slabs with and without steel fiber. Based on the finite element method, an appropriated constitutive damage model is employed to represent the nonlinear behavior of the conventional/recycled concrete, while an elastic-perfectly plastic model is used to describe the mechanical behavior of the reinforcements. To couple the independent FE meshes and incorporate the mutual interaction between the different components, rigid and non-rigid coupling technique is used to represent the perfect adherence or the bond-slip behavior. Seven concrete slabs were numerically analyzed either with different percentages of recycled aggregate replacement (0, 50 and 100%) or steel fibers content (0.0, 0.5 and 1.0%) and the results were compared with the experimental ones. The results showed that the applied methodology is capable of simulating with good accuracy the punching shear failure mechanism of the slabs. It was observed that the punching ultimate load decreased with increase of recycled aggregate content, as well as that the steel fiber addition can minimize the negative effects of recycled aggregate employment.

**Keywords:** recycled aggregate, steel fiber, punching failure, finite element, constitutive models.

**Resumo:** A utilização de resíduos da construção civil como agregado na produção de concreto vem se tomando uma alternativa cada vez mais frequente devido às vantagens associadas ao aspecto da sustentabilidade. Resultados obtidos em ensaios experimentais com concreto de agregado reciclado sugerem que propriedades mecânicas como módulo de elasticidade, resistência à compressão, tração e flexão tendem a diminuir com a substituição parcial ou total do agregado natural pelo reciclado. Por outro lado, a utilização de reforço de fibras de aço pode minimizar a redução dessas propriedades, uma vez que as fibras tendem a melhorar a resistência e a ductilidade do material. Este trabalho propõe uma abordagem numérica, buscando melhor prever e entender os comportamentos mecânicos estruturais e os modos de falha de lajes de concreto com agregado reciclado armado com e sem fibra de aço. Com base no método dos elementos finitos, um modelo constitutivo de dano apropriado é empregado para representar o comportamento não linear do concreto convencional/reciclado, enquanto que um modelo elástico-perfeitamente plástico é usado para descrever o comportamento mecânico das armaduras. Para acoplar as malhas de EF independentes e incorporar a interação mútua entre os diferentes componentes, a técnica de acoplamento rígido e não rígido é usada para representar a aderência perfeita ou o comportamento de perda de aderência (*bond-slip*). Sete lajes de concreto foram analisadas numericamente com diferentes porcentagens de substituição de agregado reciclado (0, 50 e 100%) ou teores de fibras de aço (0,0; 0,5 e 1,0%) e os resultados foram comparados com os experimentais. Os resultados mostraram que a metodologia aplicada é capaz de simular com boa precisão o mecanismo de ruptura por punção das lajes. Observou-se que a capacidade de carga à

Corresponding author: Alana Helena Cara Siqueira. E-mail: [alana.hc.siqueira@unesp.br](mailto:alana.hc.siqueira@unesp.br)**Financial support:** CAPES (Finance Code 001), CNPq (Proc.: 423379/2016-0 and 310401/2019-4) and FAPESP (Process: 2020/16789-6).**Conflict of interest:** Nothing to declare.**Data Availability:** The data that support the findings of this study are available from the corresponding author, AHCS, upon reasonable request.

This is an Open Access article distributed under the terms of the Creative Commons Attribution License, which permits unrestricted use, distribution, and reproduction in any medium, provided the original work is properly cited.

punção diminuiu com o aumento do teor de agregado reciclado, assim como que a adição de fibra de aço pode minimizar os efeitos negativos do emprego de agregado reciclado.

**Palavras-chave:** agregado reciclado, fibras de aço, falha por punção, elementos finitos, modelos constitutivos.

---

**How to cite:** A. H. C. Siqueira, M. Gimenes, O. L. Manzoli, and E. A. Rodrigues, "Numerical simulation of punching shear failure in recycled aggregate concrete slabs with steel fiber reinforcement" *Rev. IBRACON Estrut. Mater.*, vol. 16, no. 3, e16310, 2023, <https://doi.org/10.1590/S1983-41952023000300010>

## 1 INTRODUCTION

Flat reinforced concrete slabs can suffer punching shear failure under the action of concentrated load, in general, at the column location. Some conditions which influence punching behavior are slab area, position of force application, concrete compressive strength, span length, slab thickness, flexural reinforcement and supporting conditions. Due to its brittle and sudden failure mechanism, combined with environmental actions that seek to partially or totally replace the natural coarse aggregates by recycled aggregate, the punching shear failure in recycled aggregate concrete (RAC) slabs has been a topic of great interest for the scientific community, since the use of recycled aggregates can significantly reduce the mechanical properties of the concrete, contributing negatively to this failure mode [1]–[3].

Driven by some of its advantages, such as its easy molding and both relatively high compressive strength and low cost, concrete is one of the most widely used building materials, requiring a large availability of natural aggregates, around 60%–75% of the total concrete volume, whose production contributes significantly to carbon emission [4]. Another result of concrete large-scale use for decades is the large amount of waste produced by construction activities or demolitions, whose disposal also negatively contributes to the environment [5]. Thus, the use of recycled concrete aggregates (RCA), which are obtained by crushing concrete waste, brings great economic and environmental advantages, being an alternative to natural aggregates [4], [5]. However, its effects on the mechanical properties of the new recycled aggregate concrete need to be better understood. Due to its high degree of heterogeneity, recycled concrete may have lower mechanical properties than conventional concrete, such as, for example, lower compressive and tensile strengths, as well as significant reductions in the modulus of elasticity and fracture energy [6]–[9].

Seeking to overcome these disadvantages, recent studies have investigated the benefits arising from the inclusion of steel fibers in their composition, which could improve the mechanical properties of the recycled aggregate concrete [10]–[12]. As demonstrated in the studies carried out by these authors, the appropriate addition of steel fiber volumetric ratios can mitigate the disadvantages provided by the replacement percentages of recycled aggregates, such as compressive, tensile and bending strengths, providing beneficial effects on the fracture propagation process in recycled concrete. Experimental results performed by Xie et al. [13] also indicate a significant increase in flexural and tensile strength, highlighting the bridging effect provided by the fibers, which works to contain fracture initiation and propagation. Previous experiments carried out by Carneiro et al. [14] also showed similar results, as the addition of fibers resulted in the increase of all mechanical properties and better controlled the fracture propagation process in recycled concrete. The experimental studies provided by Xiao et al. [1] also show that steel fibers can improve the punching shear and energy dissipation capacities, as well as the ductility and deformations, even for the slabs with a total replacement of natural aggregate by recycled one.

Efforts have been made to develop numerical models to simulate and better understand the effects arising from both the natural aggregate and the partial or total replacement of natural aggregate by recycled aggregate, on the mechanical properties of conventional and fiber-reinforced recycled concrete [15]–[20]. In these models, more realistic geometric representations of the recycled concrete constituents can be adopted, making it possible to explicitly consider some of its heterogeneity, normally observed in the micro and mesoscopic scales, to the numerical analyses. Although this explicit representation can bring more accurate answers, the analyzes can become extremely computationally expensive, making it impossible to carry out 3D problems or perform a large number of simulations, considering varied conditions, for example, different replacement percentages of recycled aggregates. On the other hand, macroscopic models can be used, considering recycled concrete as a homogeneous material, using homogenized elastic and fracture properties (average properties), making it possible to carry out three-dimensional analyzes with much less computational time, and still bring valuable answers about the mechanical behavior of this material.

Therefore, this work proposes a numerical approach to predict and better understand the punching failure behavior of reinforced recycled aggregate concrete slabs either with different replacement percentages of recycled concrete or steel fiber volumetric ratios, which were experimentally performed by Xiao et al. [1], comparing both the experimental found in the literature [1] and numerical responses obtained. The numerical model is based on the Finite Element Method, in which regular tetrahedral finite elements are used to discretize the recycled concrete domain on the

macroscopic scale, while unidimensional finite elements are used to discretize the steel bars and fibers reinforcements. Based on the Continuum Damage Mechanics Theory (CDMT), the constitutive damage model proposed by Cervera et al. [21] is used to represent the nonlinear behavior of the recycled concrete, while an elastic-perfectly plastic model described in Simo and Hughes [22] is employed to simulate the yielding process of steel bars and fibers. To couple these independent FE meshes, the rigid and non-rigid coupling scheme proposed by Bitencourt et al. [23], [24] is properly used to respectively represent the perfect bond or the complex bond-slip phenomenon between the recycled concrete and the steel bars and fibers reinforcements. Seeking to improve the computational stability and robustness of the solution involving cracks propagation in the RAC, mechanical behavior of steel bars and fiber-RAC bond-slip relation, for all the constitutive models adopted the implicit-explicit integration scheme proposed by Oliver et al. [25] and efficiently applied for elastoplasticity problems by Prazeres et al. [26] is employed.

## 2 METHODOLOGY

The proposed 3D numerical model to simulate reinforced recycled aggregate concrete slabs with different contents of recycle aggregates and steel fibers is based on the Finite Element Method, assuming a macroscopic scale approach, in which the concrete is treated as a homogeneous material, employing homogenized material properties. The main ingredients of the numerical modeling process, formulated and implemented an *in-house* FE computer program in MATLAB®, can be divided into two parts: the FE modeling strategy, in which the tasks still in the pre-processing stage are performed; the constitutive models applied to simulate the individual mechanical behavior of the different components of the slabs (i.e. recycled concrete, steel bars and fibers and even the mutual interaction between them) that working together are able to represent the complex punching failure phenomenon of RAC slabs.

### 2.1 FE Modeling strategy

The first modeling step is to geometrically design the slab components and apply the boundary conditions (essential and natural), as illustrated in Figure 1, where due to the symmetry of problem, only a quarter of slab is numerically modeled, in which the normal displacements on the two symmetry-planes are restricted. Then, the independent FE meshes of the recycled concrete, steel bars and fibers reinforcements are generated, as illustrated in Figure 2, using the pre and post processing program GiD®, developed by CMNE (“International Center for Numerical Methods in Engineering”) of the Polytechnic University of Catalonia. The concrete domain is discretized by conventional tetrahedral finite elements and both the steel bars and fibers by one-dimensional truss elements. The support that allows upward vertical displacement is also modeled by one-dimensional bar elements.

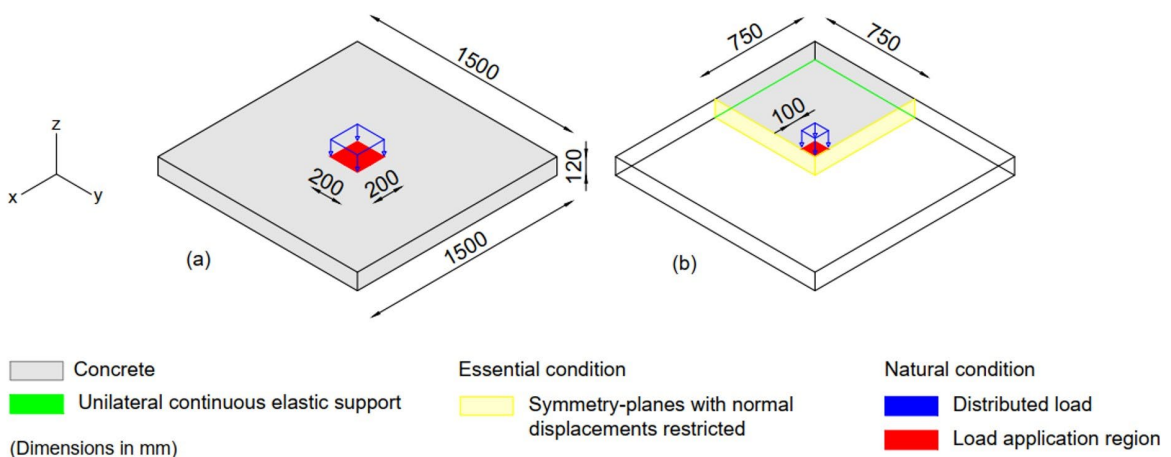


**Figure 1.** Dimensions of experimental (a) and numerically modeled slab, with its boundary conditions (b).

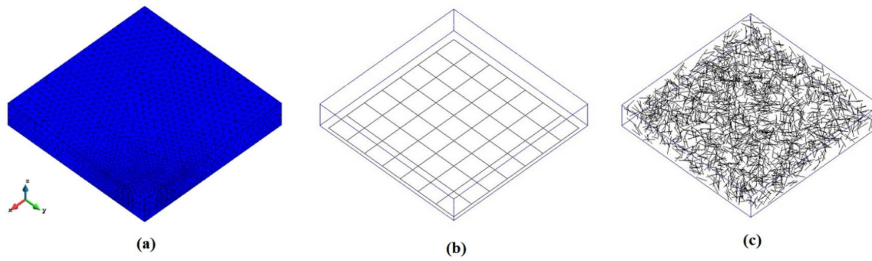


**Figure 2.** Independent meshes of concrete (a), steel bars (b) and fibers (c).

To couple these independent meshes, the coupling finite elements (CFEs) proposed by Bitencourt et al. [21] are used, as illustrated in Figure 3. These coupling elements are defined from the conventional four-nodded tetrahedral elements with an additional node that corresponds to the node of the bars or fibers, called as loose node by the authors [21], located in the domain of the corresponding tetrahedron (Figure 4). As demonstrated by the authors, the CFEs technique do not increase the number of degrees of freedom of the system and both rigid and non-rigid coupling scheme can be assumed [23], [24].

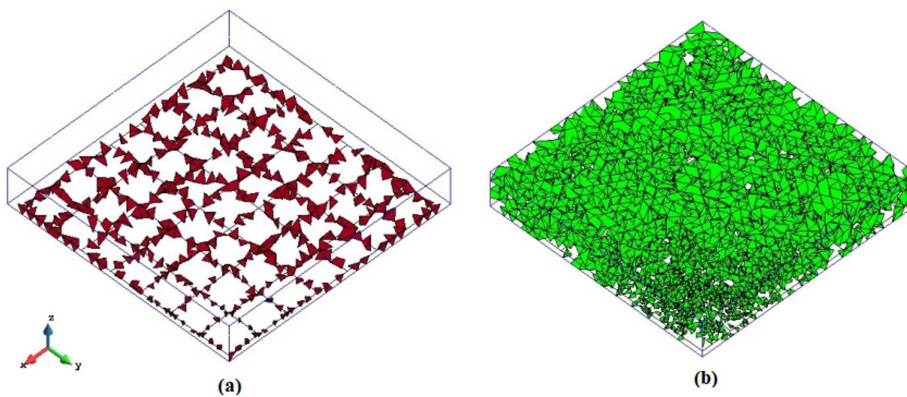


**Figure 3.** Details about the CFEs meshes used to couple the steel bars (a) and fibers (b) in the RAC mesh.

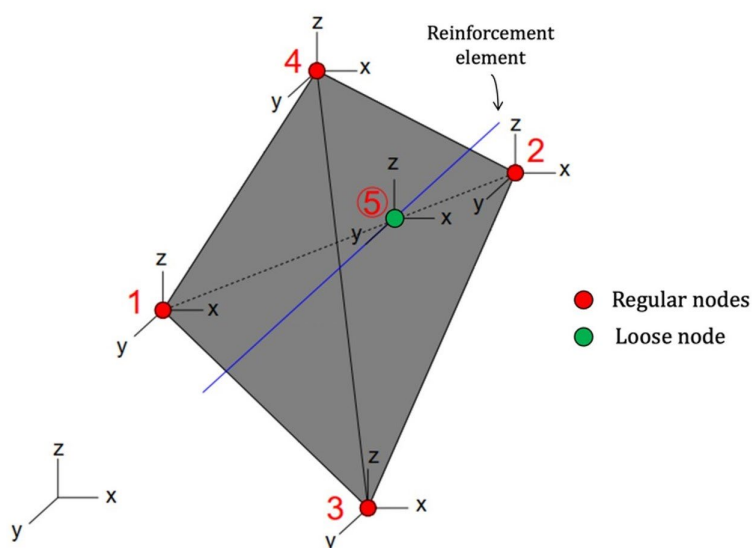


**Figure 4.** CFE defined from four-nodded tetrahedral element with the additional coupling node.

## 2.2 Constitutive models

### 2.2.1 Continuum damage model for RAC

To represent the nonlinear behavior of the RAC, the damage model proposed by Cervera et al. [21] is used, in which for the sake of simplicity the compressive behavior is assumed to be linear elastic. Thus, the effective stress tensor ( $\bar{\sigma}$ ) is split in tensile ( $\bar{\sigma}^+$ ) and compressive ( $\bar{\sigma}^-$ ) components, and only the tensile damage variable ( $d^+$ ) is defined and applied to reduce the effective tensile stress ( $\bar{\sigma}^+$ ), as described by Equation 1.

$$\sigma = (1 - d^+) \bar{\sigma}^+ + \bar{\sigma}^- \tag{1}$$

where  $0 \leq d^+ \leq 1$  and  $\sigma$  is the current stress tensor.

The equivalent effective tensile norm  $\bar{\tau}^+$  is defined according to Equation 2, as:

$$\bar{\tau}^+ = \sqrt{\bar{\sigma}^+ : \mathbf{D}_0^{-1} : \bar{\sigma}^+} \tag{2}$$

where  $\mathbf{D}_0^{-1}$  is the inverse fourth-order linear-elastic constitutive tensor.

To determine the elastic domain and the beginning of degradation growth, the damage criteria  $g^+$ (tension) is introduced by Equation 3:

$$g^+(\bar{\tau}^+, r^+) = \bar{\tau}^+ - r^+ \leq 0 \tag{3}$$

The variable  $r^+$  is the current damage thresholds and its evolution can be obtained by assuming the highest value reached by  $\bar{\tau}^+$ , as described by Equation 4.

$$r^+ = \max(r_0^+, \max(\bar{\tau}^+)) \tag{4}$$

The initial value of the initial damage thresholds  $r_0^+$  is the tensile strength of the material ( $f_t$ ).

Finally, the damage evolution rule for tension is given by Equation 5:

$$d^+ = 1 - \frac{r_0^+}{r^+} e^{A^+ (1 - \frac{r^+}{r_0^+})} \tag{5}$$

where  $A^+$  is the softening parameter derived from the fracture energy and the characteristic length.

More details about this model can be found Cervera et al. [21].

### 2.2.2 Elastoplastic model for steel bars and fibers reinforcements

To represent the mechanical behavior of the steel bars and fibers a perfect elastoplastic model is used. As illustrated in Figure 5, the stress-strain constitutive relation is based on the Young's modulus  $E_s$  and the yield stress  $f_y$  properties of the material. Details about this model can be found in Simo and Hughes [22].

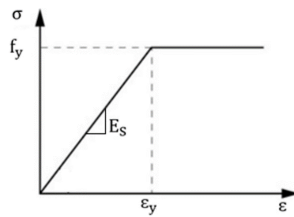


Figure 5. Perfect elastoplastic model assumed for the bars and fibers.

### 2.2.3 CFE model for bars and fibers reinforcements-RAC interactions

To represent the mutual interaction between the reinforcements (steel bars and fibers) and the RAC, the rigid and non-rigid coupling technique proposed by Bitencourt et al. [23], [24] is used, which has also recently been used to couple non-conforming meshes in multiscale concrete approaches [27]–[29].

According to this technique, in which independent FE meshes can be assumed, the reinforcement contribution is added according to the global internal force vector ( $\mathbf{F}^{int}$ ) and stiffness matrix ( $\mathbf{K}$ ) presented in Equations 6 and 7.

$$\mathbf{F}^{int} = \underbrace{\mathbf{A}_{e=1}^{nel\Omega^C} \mathbf{F}_{e,\Omega^C}^{int}}_{\text{concrete elements}} + \underbrace{\mathbf{A}_{e=1}^{nel\Omega^B} \mathbf{F}_{e,\Omega^B}^{int}}_{\text{bars}} + \underbrace{\mathbf{A}_{e=1}^{nel\Omega^F} \mathbf{F}_{e,\Omega^F}^{int}}_{\text{fibers}} + \underbrace{\mathbf{A}_{e=1}^{nel\Omega^{CFE}} \mathbf{F}_{e,\Omega^{CFE}}^{int}}_{\text{coupling elements}} \tag{6}$$

$$\mathbf{K} = \underbrace{\mathbf{A}_{e=1}^{nel\Omega^C} \mathbf{K}_{e,\Omega^C}}_{\text{concrete elements}} + \underbrace{\mathbf{A}_{e=1}^{nel\Omega^B} \mathbf{K}_{e,\Omega^B}}_{\text{bars}} + \underbrace{\mathbf{A}_{e=1}^{nel\Omega^F} \mathbf{K}_{e,\Omega^F}}_{\text{fibers}} + \underbrace{\mathbf{A}_{e=1}^{nel\Omega^{CFE}} \mathbf{K}_{e,\Omega^{CFE}}}_{\text{coupling elements}} \tag{7}$$

In these equations  $\mathbf{A}$  is the conventional FE assembly operator. The first, second and third terms are related to the respective independent FE meshes of the RAC, steel bars and fibers. The fourth term is associated with the CFE scheme.

As demonstrated by the authors [23], [24] this technique can be used to represent rigid coupling (perfect bond) between the reinforcements and the RAC. In this case, it is sufficient to assume a linear relationship between reaction force,  $\mathbf{F}$ , and relative displacement,  $[\mathbf{U}]$ , described in Equation 8, and assume high values for the penalty parameters  $\tilde{C}$  presented in Equation 9.

$$\mathbf{F} = \mathbf{C}[\mathbf{U}] \tag{8}$$

$$\mathbf{C} = \begin{bmatrix} \tilde{C} & 0 & 0 \\ 0 & \tilde{C} & 0 \\ 0 & 0 & \tilde{C} \end{bmatrix} \tag{9}$$

On the other hand, a non-rigid coupling can be considered, in which the complex bond-slip phenomenon between reinforcements and RAC is explicitly simulated. Thus, the relationship described in Equation 8 is now governed by an appropriate constitutive damage model with a hardening/softening law formulated to properly describe the bond-slip curve proposed by CEB *Fib* Model Code [30] (See Figure 6), in which the shear stress ( $\tau$ ) as a function of the relative displacement ( $s$ ) for monotonic pullout test is given by Equation 10.

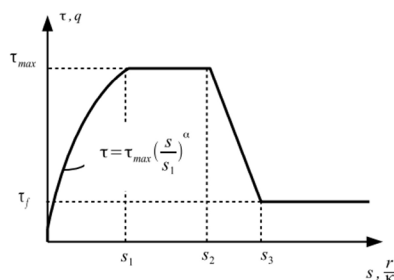


Figure 6. Interface stress bond-slip relationship (monotonic loading) proposed by CEB *Fib* Model Code [30].

$$\tau(s) = \begin{cases} \tau_{max} \left(\frac{s}{s_1}\right)^\alpha & \text{if } s \leq s_1 \\ \tau_{max} & \text{if } s_1 \leq s \leq s_2 \\ \tau_{max} - \frac{(\tau_{max}-\tau_f)(s-s_2)}{(s_3-s_2)} & \text{if } s_2 \leq s \leq s_3 \\ \tau_f & \text{if } s > s_3 \end{cases} \quad (10)$$

It is important to note that  $\alpha$ , maximum shear stress  $\tau_{max}$ , residual shear stress  $\tau_f$  and the relative displacements  $s_i$  ( $i = 1, 2, 3$ ) are parameters associated with concrete strength ( $f_{ck}$ ), bar geometry, confining situation and bond condition [30]. More details description of this model can be found in Bitencourt et al. [23], [24].

For the sake of simplicity, in the proposed approach a rigid coupling (perfect-bond) between the steel bars and RAC is assumed, while the described non-rigid coupling is used to represent the bond-slip behavior between the steel fibers and the RAC.

### 3 NUMERICAL SIMULATIONS

The numerical modeling performed in this study was based on the experimental tests proposed by Xiao et al. [1], in which a series of reinforced concrete slabs with different contents of recycled coarse aggregate and steel fibers were tested in laboratory, in order to investigate the complex punching shear behavior. The natural coarse aggregates were gravel stones, and the recycled coarse aggregates used came from the demolition of concrete with average compressive strength of 30 MPa, with diameter size dimensions varying from 5 to 15 mm and from 15 to 25 mm. The steel fibers were wire-type shaped with angles on both ends, average length of 50 mm, diameter of 0.9 mm, with volumetric ratios of 0.5% (39.3 kg/m<sup>3</sup>) and 1.0% (78.5 kg/m<sup>3</sup>) being used. The reinforcements were hot-rolled ribbed bars, with 12 mm diameter, 100 mm apart with reinforcement ratio of 1.142%. The slabs were positioned in a reinforced concrete frame with an angle steel frame in four simply-supported edges boundary conditions, applying concentrated load with constant speeds, until the complete failure of the slabs.

In this paper, the slabs numerically simulated are: 0% (RAC0), 50% (RAC50-0%) and 100% (RAC100-0%) of recycled aggregate replacement with bars and without fibers; 50% of recycled aggregate with bars and varying the amount of fibers in 0.5% and 1% (SFRAC50-0.5% and SFRAC50-1%, respectively) and 100% of recycled aggregate, with bars varying the fiber content in 0.5% and 1%. (SFRAC100-0.5% and SFRAC100-1%, respectively).

The numerical parameters used are presented in Table 1. The Young's modulus was provided by the experimental results [1] and the Poisson's ratio, as its value was not informed in the experiment, the typical value of 0.2 was adopted. The average tensile strength ( $f_{ct,m}$ ) was obtained by Equation 11 (NBR 6118 [31]), for concrete classes up to C50:

$$f_{ct,m} = 0,3 f_{ck}^{\frac{2}{3}} \quad (11)$$

where  $f_{ck}$  is the characteristic compressive strength of concrete.

The value of fracture energy ( $G_F$ ) was given by Equation 12, according to CEB *Fib* Model Code [30].

$$G_F = G_{F0} \left(\frac{f_{cm}}{10}\right)^{0,7} \quad (12)$$

where  $f_{cm}$  is the average compressive strength and  $G_{F0}$  is constant, determined by the maximum diameter of the coarse aggregates (CEB *Fib* Model Code [30]). The aggregates in the experiment had a maximum diameter of 25 mm. Thus, the value  $G_{F0} = 0.04575$  Nmm/mm<sup>2</sup> is used.

**Table 1.** Parameters assumed for the RAC.

Specimen	Modulus of elasticity (MPa) (x 10 <sup>4</sup> )	Tensile strength (MPa)	Fracture energy (N/mm)	Poisson Ratio
RAC0	3.73	3.50	0.1205	0.2
RAC50-0%	2.96	3.10	0.1061	0.2
SFRAC50-0,5%	2.96	3.10	0.1061	0.2
SFRAC50-1%	2.96	3.10	0.1061	0.2
RAC100-0%	2.74	2.80	0.0952	0.2
SFRAC100-0,5%	2.74	2.80	0.0952	0.2
SFRAC100-1%	2.74	2.80	0.0952	0.2

For the steel bars and fibers the perfect elastoplastic model described in subsection (2.2.2) is used, assuming the same Young’s modulus of  $E_s = 200 \text{ GPa}$  and yield strength of  $f_y = 390 \text{ MPa}$  for both. According to the models presented in subsection (2.2.3), a perfect bond between the steel bars and RAC is considered by using the penalty parameter value of  $\tilde{C} = 10^7 \text{ N/mm}$ , while a bond-slip between the steel fibers and RAC is modeled by assuming  $\tau_{max} = 8.50 \text{ MPa}$ ,  $\tau_f = 4.50 \text{ MPa}$ ,  $S_1 = 0.01 \text{ mm}$ ,  $S_2 = 0.01 \text{ mm}$ ,  $S_3 = 6.50 \text{ mm}$  and  $\alpha = 0.4$ .

One-dimensional finite elements (truss elements) with linear elastic model only in compression were used to model the interaction between the slabs and the unilateral continuous elastic support, in which the loss of contact between them can occur freely.

The stiffness was obtained by multiplying the influence area by the support reaction modulus of  $0.4 \text{ MPa/mm}$ , that showed to be an adequate value to represent the reinforced concrete frame with an angle steel frame and also the initial stiffness of the numerical curves.

In all analyzes performed the load was incrementally applied in 1500 steps, controlling the vertical displacement in  $0.04 \text{ mm}$  per step.

### 3.1 Concrete with 0%, 50% and 100% of recycled aggregates without fibers

Herein the numerical responses written in terms of the Force vs. displacements curves are compared against the experimental developed by Xiao et al. [1] for the reinforced concrete slabs with 0% (reference concrete), 50% and 100% of recycled aggregates with conventional steel bars and without fibers, as well as the failure pattern, are presented.

Figure 7 illustrates both the numerical and experimental curves obtained for the reference concrete (RAC0). In general, the numerical responses reproduced well some notable experimental results aspects, especially the ultimate load and the typical punching failure pattern (punching cone formation) shown in Figures 8 and 9. In Figure 8 the displacement field in the vertical direction (z-direction) is showed, while in Figure 9a-e the tensile damage distribution is presented, in which the mentioned punching failure propagation process can be observed for different loading steps. In the initial stage of loading no crack occurs. With increasing load, it is possible to notice that cracks propagate radial to the slab from the applied load location to the edge (Figure 9a-c). At more advanced levels of loading, it is possible to observe the formation of curved cracks around the loading area (Figure 9d and 9e), which agrees with the experimental results reported by Xiao et al. [1].

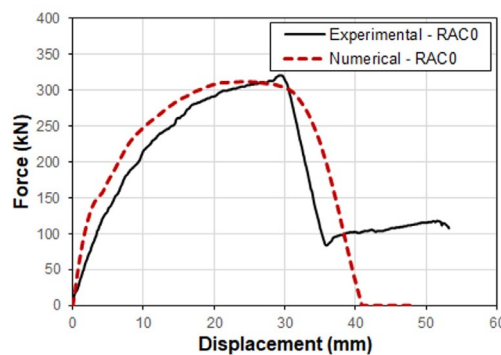


Figure 7. Force x displacement curves of RAC0 slabs.

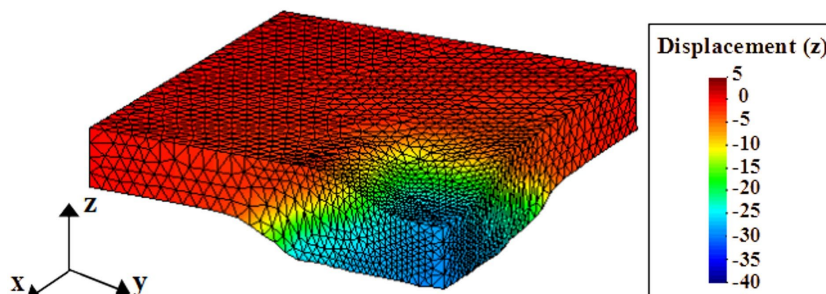


Figure 8. Deformed configuration (scaling factor of 2 times) with the displacement field (in mm) of RAC0 slab, at the end of loading.

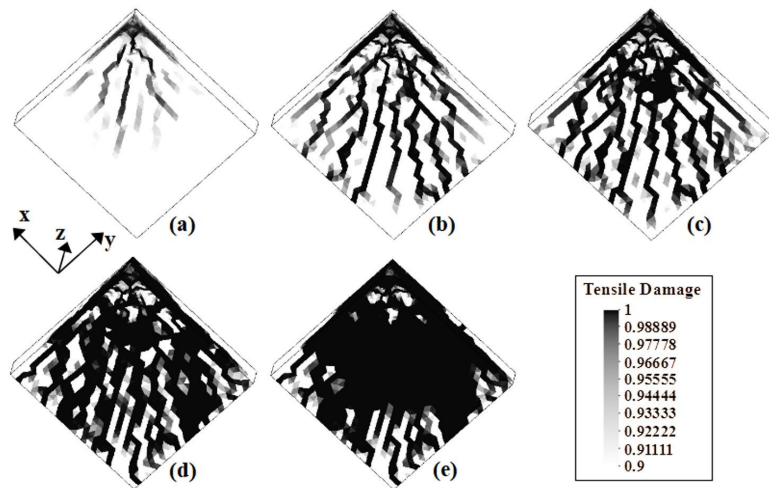


Figure 9. Tensile damage distribution obtained for different loading steps: (a) 100, (b) 300, (c) 500, (d) 1000 and (e) 1500.

The numerical force-displacements curves for the recycled concrete with 50% and 100% of recycled aggregates are plotted with the experimental curves in Figure 10a and 10b. It is possible to note that the responses obtained with the proposed methodology are in good agreement with the results found in the literature [1]. The deformed configurations (scaling factor of 2 times the original one) with the displacement fields in the z-directions of these slabs are illustrated in Figure 11, in which the punching failure patterns with an oblique cone formation can also be observed.

The numerical curves obtained for the three replacement percentages of recycled aggregates are presented in Figure 12. It is worth noting how the peak-load (punching ultimate load) and the energy dissipation are reduced as the percentage of recycled aggregates is increased, showing that the applied methodology can reproduce well the recycled aggregate effect by reducing the homogenized fracture properties as the recycled aggregate content is increased.

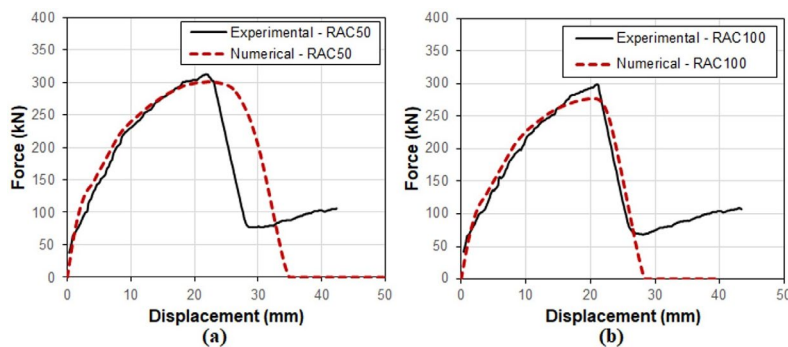


Figure 10. Force x displacement curves of (a) RAC50 and (b) RAC100 slabs.

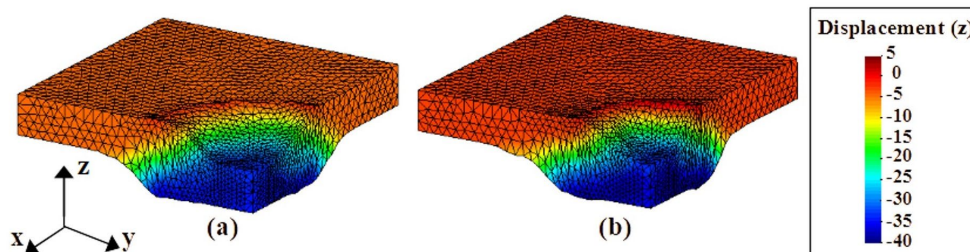


Figure 11. Deformed shapes (scaling factor of 2 times) with the displacement fields (in mm) of the (a) RAC50 and (b) RAC100 slabs, at the end of loading.

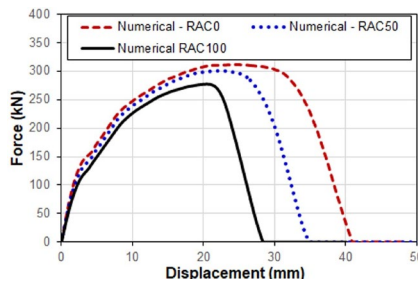


Figure 12. Numerical force x displacement curves of RAC0, RAC50 and RAC100 slabs.

### 3.2 Concrete with 50% of recycled aggregates and 0.5% and 1.0% of fibers

This section presents the numerical results obtained for the recycled concrete with 50% of replacement of recycled coarse aggregates, assuming 0.5% and 1.0% of steel fibers. Figure 13a and 13b illustrates the numerical force-displacement curves obtained compared with the experimental responses provided by Xiao et al. [1]. Comparing the plotted results it is worthy to note how the proposed approach can reproduce the experimental results, as well as how the addition of fibers is able to mitigate the disadvantages provided by the replacement of natural by recycled aggregates, as it can be proven in Figure 14, in which both numerical curves showed in this section are compared against the experimental one obtained for the reference concrete (RAC0) showed in section 3.1. The mentioned advantages may be related to the bridging effect provided by the fibers, which works to contain fracture initiation and propagation, as described by Xie et al. [13]. It is important to point out that these same beneficial effects on the mechanical properties of the RAC produced by the addition of fiber were observed in experimental studies obtained by other authors [10] [11] [12]. In Figure 15a-c it is possible to observe the tensile stress field of the fibers for different loading steps, which work to prevent crack propagation in the RAC and, consequently, contributing to the reduction of the drawbacks of replacement of the natural aggregates by the recycled aggregates.

Figure 16a-d shows the distribution of the tensile damage variable at step 1000 in two different views for the slabs with 0.5% (Figure 16a and 16c) and 1.0% (Figure 16b and 16d) of steel fibers. It is important to note that in both analyzes the oblique cone formation is observed. However, with the increasing of steel fibers volumetric ratio the cut cone integrity is improved, as illustrated in Figure 16c and 16d, in which the initial transition process of the punching failure pattern to bending-punching failure pattern is observed, in agreement with the experimental results.

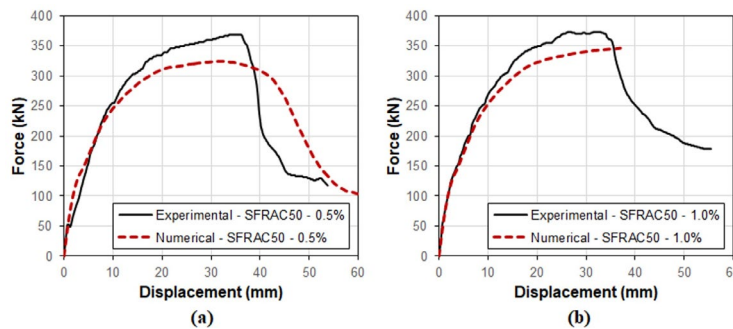


Figure 13. Force x displacement curves of (a) SFRAC50-0.5% and (b) SFRAC50-1.0% slabs.

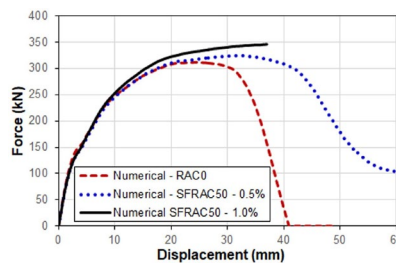


Figure 14. Numerical force x displacement curves obtained for slabs with RAC0, SFRAC50-0.5% and SFRAC50-1.0%.

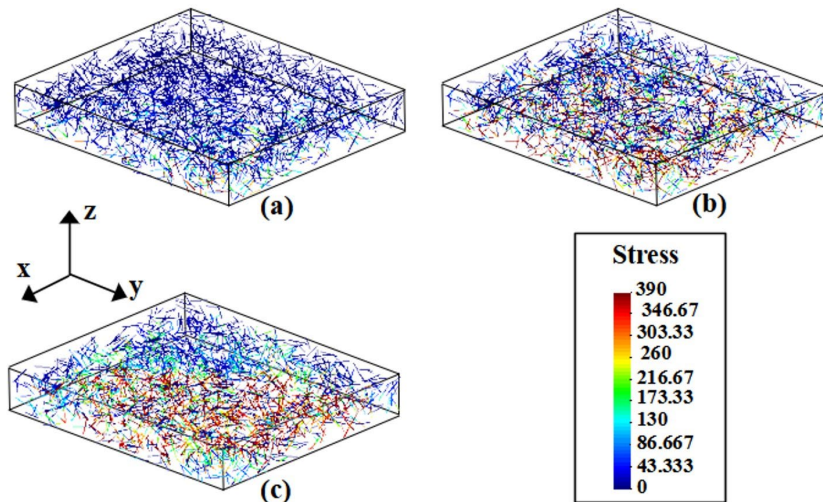


Figure 15. Tensile stress field obtained for the fibers for different loading steps: (a) 100, (b) 500 and (c) 1500.

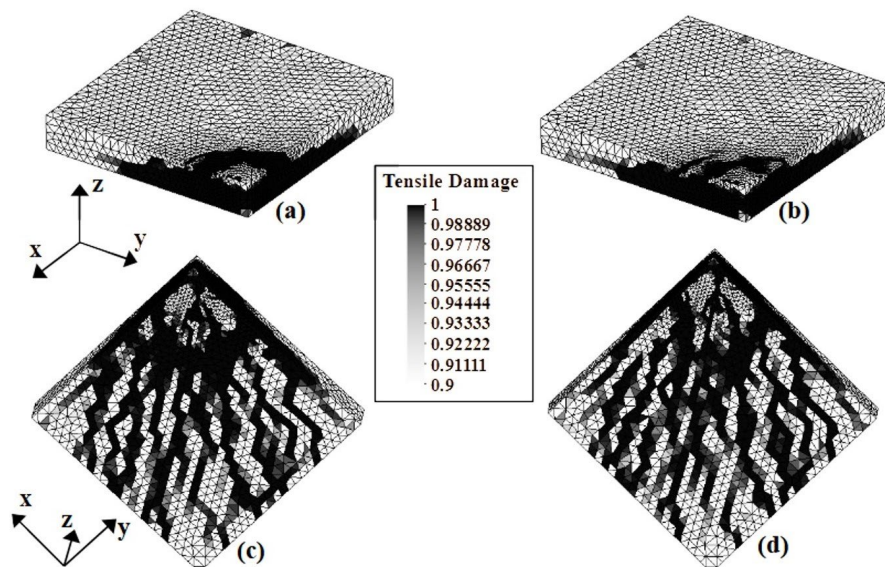


Figure 16. Tensile damage distribution in two different views at step 1000 for slabs with 50% of recycled aggregates and steel fiber volumetric ratios of 0.5% (a and c) and 1.0% (b and d).

### 3.3 Concrete with 100% of recycled aggregates and 0.5% and 1.0% of fibers

Figure 17a and 17b illustrates the numerical force-displacement curves obtained compared against the experimental responses provided by Xiao et al. [1]. Again, the numerical responses were able to represent well the experimental responses, as well as the beneficial effects produced by the addition of steel fibers, that is, reducing the drawbacks caused by the complete replacement of the natural aggregates by the recycled aggregates, as it can also be seen in both numerical curves obtained in this section, plotted with the curve obtained for the reference concrete in section 3.1, illustrated in Figure 18. Note that, with the increasing of steel fibers volumetric ratio, the punching ultimate load is improved. Also note that even for the total replacement of the natural aggregate, the numerical responses with the addition of fibers show better results than that obtained for the reference concrete, such as the ultimate load, ductility, and energy consumption. However, the punching failure patterns with the cut oblique cone formations are still observed by the distribution of the tensile damage variable illustrated in Figure 19a-d. However, for the steel fiber volumetric ratio of 1.0%, again the transition process of the punching failure pattern to bending-punching failure pattern is noted.

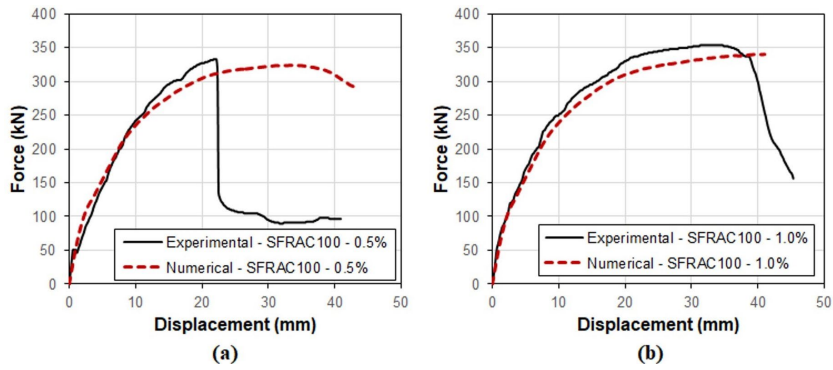


Figure 17. Force x displacement curves of (a) SFRAC100-0.5% and (b) SFRAC100-1.0% slabs.

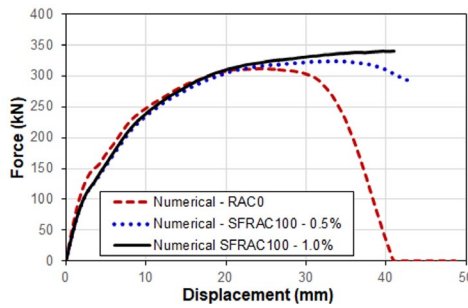


Figure 18. Numerical force x displacement curves obtained for slabs with RAC0, SFRAC100-0.5% and SFRAC100-1.0%.

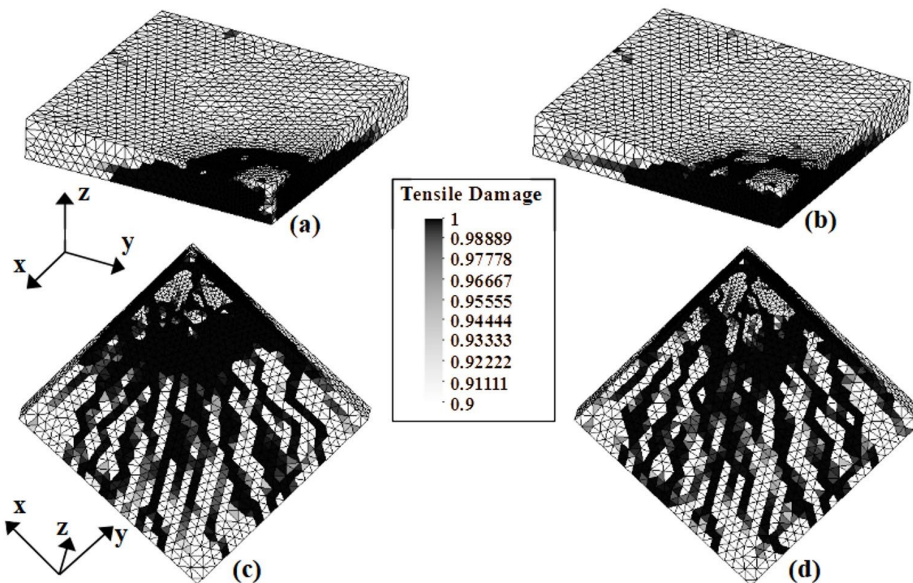


Figure 19. Tensile damage distribution in two different views at step 1000 for slabs with 100% of recycled aggregates and steel fiber volumetric ratios of 0.5% (a and c) and 1.0% (b and d).

#### 4 CONCLUSIONS

In the present paper a numerical approach implemented into an *in-house* finite element code has been proposed to simulate and to better understanding the punching failure behavior of reinforced concrete slabs (i) without fibers with only natural coarse aggregates (natural/reference concrete) and with recycled aggregate replacement percentages of 50% and 100%, and (ii) also using different steel fibers volumetric ratios of 0.5% and 1.0% for slabs with recycled aggregates. To simulate the nonlinear

behavior of the natural and recycled concrete the constitutive damage model proposed by Cervera et al. [21] was used, while an elastic-perfectly plastic model found in Simo and Hughes [22] was used to represent the mechanical behavior of the reinforcing steel bars and fibers. The coupling scheme proposed by Bitencourt et al. [23], [24], either to simulate the perfect-bond (rigid coupling) between the steel bars and recycled concrete or to model the complex bond-slip phenomenon (non-rigid coupling) defined by the CEB *Fib* Model Code [30] between the steel fiber and recycled concrete, was also properly implemented. To improve the stability and robustness of the solution involving cracks propagation in the RAC, mechanical behavior of steel bars and the fiber-RAC bond-slip relation, the implicit-explicit integration scheme (Impl-Ex) proposed by Oliver et al. [25] was employed for all these constitutive models adopted.

In this context, the slabs described above were simulated, in which the qualitative and quantitative numerical results obtained presented good agreement with the experimental responses provided by Xiao et al. [1]. For the slabs without fibers, with the increase of the recycled aggregate replacement percentages, the punching ultimate load is reduced, as well as the ductility and the energy consumption. The punching failure pattern was observed, with both integrity reduced and formation of a more pronounced oblique cone, as the percentage of recycled aggregate is increased. On the other hand, with the addition and increase of steel fiber volumetric ratio, the punching ultimate load, the ductility and energy consumption were improved, mitigating the disadvantages provided by the replacement of natural aggregate by recycled one, and even showing better results than that obtained for the reference concrete, proving to be in full agreement with the experimental results found in the literature [1] and [10]–[12].

Therefore, based on the good numerical results obtained, it can be highlighted that the proposed approach to simulate the punching failure behavior of reinforced concrete slabs is very efficient, and can provide valuable answers about this failure mechanism, mainly in the presence of alternative materials such as recycled aggregate and fibers. It is also important to highlight that the different materials can be discretized in a completely independent way. Furthermore, the constitutive models used are relatively simple and easy to be implemented in conventional FE programs, which used together are able to efficiently represent the complex punching failure phenomenon.

## ACKNOWLEDGEMENTS

The authors wish to acknowledge the financial support of the National Council for Scientific and Technological Development – CNPq (Proc.: 423379/2016-0 and 310401/2019-4), Coordination for the Improvement of Higher Education Personnel – CAPES (Finance Code 001) and São Paulo Research Foundation (FAPESP) (Process: 2020/16789-6).

## REFERENCES

- [1] J. Xiao, W. Wang, Z. Zhou, and M. M. Tawana, "Punching shear behavior of recycled aggregate concrete slabs with and without steel fibres," *Front. Struct. Civ. Eng.*, vol. 13, no. 3, pp. 725–740, Jun 2019, <http://dx.doi.org/10.1007/s11709-018-0510-6>.
- [2] H. Marzouk and A. Hussein, "Experimental investigation on the behavior of high-strength concrete slabs," *ACI Mater. J.*, vol. 88, no. 6, pp. 701–713, 1991.
- [3] S. Guandalini, O. L. Burdet, and A. Muttoni, "Punching tests of slabs with low reinforcement ratios," *ACI Mater. J.*, vol. 106, no. 1, pp. 87–95, 2009.
- [4] T. R. Sonawane and S. S. Pimplikar, "Use of recycled aggregate in concrete," *Int. J. Eng. Res. Technol.*, vol. 2, no. 1, pp. 1–9, 2013.
- [5] M. Malešev, V. Radonjanin, and S. Marinković, "Recycled concrete as aggregate for structural concrete production," *Sustainability*, vol. 2, no. 5, pp. 1204–1225, 2010, <http://dx.doi.org/10.3390/su2051204>.
- [6] M. Casuccio, M. Torrijos, G. Giaccio, and R. Zerbino, "Failure mechanism of recycled aggregate concrete," *Constr. Build. Mater.*, vol. 22, no. 7, pp. 1500–1506, 2008, <http://dx.doi.org/10.1016/j.conbuildmat.2007.03.032>.
- [7] A. E. B. Cabral, V. Schalch, D. C. C. Dal Molin, and J. L. D. Ribeiro, "Mechanical properties modeling of recycled aggregate concrete," *Constr. Build. Mater.*, vol. 24, no. 4, pp. 421–430, Apr 2010, <http://dx.doi.org/10.1016/j.conbuildmat.2009.10.011>.
- [8] J. Brito and N. Saikia, *Recycled Aggregate in Concrete: Use of Industrial, Construction and Demolition Waste*. New York: Springer, 2013.
- [9] B. S. Hamad and A. H. Dawi, "Sustainable normal and high strength recycled aggregate concretes using crushed tested cylinders as coarse aggregates," *Case Stud. Constr. Mater.*, vol. 7, pp. 228–239, Dec 2017, <http://dx.doi.org/10.1016/j.cscm.2017.08.006>.
- [10] N. V. Ramana, "Performance of crimped steel fibre reinforced recycle aggregate concrete," *Int. J. Adv. Technol. Eng. Sci.*, vol. 4, no. 1, pp. 152–159, 2016.
- [11] Y. Paluri, S. Mogili, H. Mudavath, and V. Noolu, "Effect of fibres on the strength and toughness characteristics of recycled aggregate concrete," *Mater. Today Proc.*, vol. 38, pp. 2537–2540, 2021, <http://dx.doi.org/10.1016/j.matpr.2020.07.555>.

- [12] S. Jahandari et al., "Mechanical properties of recycled aggregate concretes containing silica fume and steel fibres," *Materials*, vol. 14, no. 22, pp. 7065, Nov 2021, <http://dx.doi.org/10.3390/ma14227065>.
- [13] J. Xie, S. Kou, H. Ma, W.-J. Long, Y. Wang, and T.-H. Ye, "Advances on properties of fiber reinforced recycled aggregate concrete: Experiments and models," *Constr. Build. Mater.*, vol. 277, pp. 122345, Mar 2021, <http://dx.doi.org/10.1016/j.conbuildmat.2021.122345>.
- [14] J. A. Carneiro, P. R. L. Lima, M. B. Leite, and R. D. Toledo Filho, "Compressive stress-strain behavior of steel fiber reinforced-recycled aggregate concrete," *Cement Concr. Compos.*, vol. 46, pp. 65–72, Feb 2014, <http://dx.doi.org/10.1016/j.cemconcomp.2013.11.006>.
- [15] Y. Peng, H. Chu, and J. Pu, "Numerical simulation of recycled concrete using convex aggregate model and base force element method," *Adv. Mater. Sci. Eng.*, vol. 2016, pp. 1–10, 2016., <http://dx.doi.org/10.1155/2016/5075109>.
- [16] E. A. Rodrigues, O. L. Manzoli, L. A. Bitencourt Jr., and T. N. Bittencourt, "2D mesoscale model for concrete based on the use of interface element with a high aspect ratio," *Int. J. Solids Struct.*, vol. 94-95, pp. 112–124, 2016, <http://dx.doi.org/10.1016/j.ijsolstr.2016.05.004>.
- [17] M. Guo, F. Grondin, and A. Loukili, "Numerical analysis of the failure of recycled aggregate concrete by considering the random composition of old attached mortar," *J. Build. Eng.*, vol. 28, pp. 101040, Mar 2020, <http://dx.doi.org/10.1016/j.jobbe.2019.101040>.
- [18] N. Kachouh, T. El-Maaddawy, and H. El-Hassan, "Numerical modelling of steel fiber recycled aggregate concrete deep beams," in *Proc. 5th World Congr. Civil Struct. Environ. Eng. (CSEE'20)*, Avestia, 2020. (Virtual Conference).
- [19] E. A. Rodrigues, M. Gimenes, L. A. Bitencourt Jr, and O. L. Manzoli, "A concurrent multiscale approach for modeling recycled aggregate concrete," *Constr. Build. Mater.*, vol. 267, pp. 121040, Jan 2021, <http://dx.doi.org/10.1016/j.conbuildmat.2020.121040>.
- [20] M. Gimenes, E. A. Rodrigues, L. A. Bitencourt Jr, and O. L. Manzoli, "2D mesoscale modeling of compressive fracture in concrete using a mesh fragmentation technique," *Int. J. Solids Struct.*, vol. 260-261, pp. 112031, 2023. <http://dx.doi.org/10.1016/j.ijsolstr.2022.112031>
- [21] M. Cervera, J. Oliver, and O. Manzoli, "A rate-dependent isotropic damage model for the seismic analysis of concrete dams," *Earthquake Eng. Struct. Dynam.*, vol. 25, no. 9, pp. 987–1010, Sep 1996, [http://dx.doi.org/10.1002/\(SICI\)1096-9845\(199609\)25:9<987::AID-EQE599>3.0.CO;2-X](http://dx.doi.org/10.1002/(SICI)1096-9845(199609)25:9<987::AID-EQE599>3.0.CO;2-X).
- [22] J. C. Simo and T. J. R. Hughes, *Computational Inelasticity*. New York: Springer-Verlag, 1998.
- [23] L. A. G. Bitencourt Jr., O. L. Manzoli, P. G. C. Prazeres, E. A. Rodrigues, and T. N. Bittencourt, "A coupling technique for non-matching finite element meshes," *Comput. Methods Appl. Mech. Eng.*, vol. 290, pp. 19–44, Jun 2015, <http://dx.doi.org/10.1016/j.cma.2015.02.025>.
- [24] L. A. G. Bitencourt Jr., O. L. Manzoli, Y. T. Trindade, E. A. Rodrigues, and D. Dias-da-Costa, "Modeling reinforced concrete structures using coupling finite elements for discrete representation of reinforcements," *Finite Elem. Anal. Des.*, vol. 149, pp. 32–44, Sep 2018, <http://dx.doi.org/10.1016/j.finel.2018.06.004>.
- [25] J. Oliver, A. Huespe, and J. Cante, "An implicit/explicit integration scheme to increase computability of non-linear material and contact/friction problems," *Comput. Methods Appl. Mech. Eng.*, vol. 197, no. 21-24, pp. 1865–1889, 2008, <http://dx.doi.org/10.1016/j.cma.2007.11.027>.
- [26] P. G. Prazeres, L. A. Bitencourt Jr., T. N. Bittencourt, and O. L. Manzoli, "A modified implicit–explicit integration scheme: an application to elastoplasticity problems," *J. Braz. Soc. Mech. Sci. Eng.*, vol. 38, no. 1, pp. 151–161, 2016, <http://dx.doi.org/10.1007/s40430-015-0343-3>.
- [27] E. A. Rodrigues, O. L. Manzoli, L. A. Bitencourt Jr., T. N. Bittencourt, and M. Sánchez, "An adaptive concurrent multiscale model for concrete based on coupling finite elements," *Comput. Methods Appl. Mech. Eng.*, vol. 328, pp. 26–46, 2018, <http://dx.doi.org/10.1016/j.cma.2017.08.048>.
- [28] E. A. Rodrigues, O. L. Manzoli, and L. A. Bitencourt Jr., "3D concurrent multiscale model for crack propagation in concrete," *Comput. Methods Appl. Mech. Eng.*, vol. 361, pp. 112813, 2020, <http://dx.doi.org/10.1016/j.cma.2019.112813>.
- [29] M. Gimenes, E. A. Rodrigues, M. A. Maedo, L. A. Bitencourt Jr., and O. L. Manzoli, "2D crack propagation in high-strength concrete using multiscale modeling," *Multiscale Sci. Eng.*, vol. 2, no. 2-3, pp. 169–188, 2020, <http://dx.doi.org/10.1007/s42493-020-00049-y>.
- [30] International Federation for Structural Concrete, *fib Model Code for Concrete Structures 2010*. Lausanne: Ernst & Sohn, 2013.
- [31] Associação Brasileira de Normas Técnicas. *Design of Concrete Structures – Procedure*, ABNT NBR 6118, 2014 (in Portuguese).

---

**Author contributions:** AHCS and MG: formal analysis, methodology, validation, visualization, writing-original draft; OLM and EAR: conceptualization, supervision, writing-review, editing & data curation.

**Editors:** Leandro Trautwein, Mauro Real, Mario Pimentel.